Eight week report for IASc-INSA-NASI Summer Research Fellowship

on

Study of Pulsar Emission Mechanism using GMRT

Name: Komal Gupta

Application Number: PHYS2021

Guide: Prof. Yashwant Gupta

At

National Centre for Radio Astrophysics - TIFR, Pune

Pune University Campus, Post Bag 3,

Ganeshkhind, Pune - 411007, India

Abstract

Owing to its high sensitivity and extensive frequency coverage, the GMRT allows study of individual pulses of pulsars. Individual pulses show a variety of structures over a range of timescales, which reveals a wealth of information about the emission process. These pulses have been observed to consist of one or more subpulses, which further show quasi-periodic intensity fluctuations known as microstructures. Furthermore, the pulse intensity often drops to a low value for a few pulses and then abruptly returns to normal. This phenomenon, known as nulling, is inversely correlated with the age of the pulsar. In this project, we try to explain the underlying emission mechanism through a detailed analysis of individual pulse data from several pulsars. The raw data obtained from the GMRT is processed by making use of the software package GPTool. The output from GPTool is analyzed to obtain the intensity profile for individual pulses which are then scanned for the presence of microstructures and pulse nulling. The analysis is performed for several normal pulsars, as well as a few millisecond pulsars which can be observed using the GMRT.

Contents

List of Figures

1 Introduction

A pulsar is a highly magnetized, rotating neutron star that emits beams of electromagnetic radiation. As the beam sweeps past the observer's line of sight once per rotation, regularly spaced pulses are obtained. Since their discovery by Jocelyn Bell-Burnell and Antony Hewish at Cambridge in 1967, pulsars have provided us a wealth of information about neutron star physics, general relativity and the interstellar medium. Much of our knowledge of the underlying emission mechanism is derived from radio pulsar observations, which have been extensive over the past few decades.

1.1 Background

While the radiation emitted by pulsars is spread over the entire spectrum, the earth's atmosphere permits only optical and radio frequencies to reach the surface. The frequencies observed via surface telescopes is therefore constrained to these bands. Pulsars are relatively weak radio sources, and highly sensitive radio telescopes with baselines of the order of several kilometers are required to resolve them. Individual pulses are observable from only the strongest sources, and most pulsars require the coherent addition of several pulses together in a process known as folding. The integrated pulse profile thus obtained can be considered as a signature of the pulsar at the frequency of observation.

Individual pulses consist of one or more subpulses, each with an approximately Gaussian shape. In certain pulsars, subpulses drift systematically over the window defined by the integrated profile. Individual pulse data also shows evidence of pulse nulling, which is when the mean intensity over the pulse window abruptly drops to a low value for some pulses before returning to normal. The study of these phenomena can provide us with information about the physical processes that lead to one of the most precise clocks in the universe.

1.2 Motivation

Pulsar astronomy currently is enjoying one of the most productive stages in its relatively short existence. Most new discoveries are being made using the 64-m Parkes telescope, whose scientific output dominates the flood of new pulsars being found. Other highly sensitive instruments, in particular the Green Bank Telescope, the upgraded Giant Meterwave Radio Telescope and the upgraded Arecibo telescope are being used to perform deep targeted searches for pulsars in supernova remnants and globular clusters.

Individual pulse studies are relatively difficult to conduct due to broadening effects such as dispersion and scattering. Consequently, single pulses have been observed for only the brightest sources. In order to detect single pulses, highly sensitive instruments are required to obtain data with sufficient signal-to-noise ratios (SNRs). Moreover, one needs to be able to correct for dispersive effects of the interstellar medium via dedispersion. Even though these phenomena are quite common, most previous studies concentrated on characterizing drifting and nulling behavior at a single observing frequency. Studying the behavior at two or more frequencies simultaneously allows us to explore possible correlations between the emission

process and observing frequency. A multi-frequency study also helps in establishing a broadband nature of the phenomena. Owing to its high sensitivity and extensive frequency coverage, the upgraded GMRT provides a unique opportunity to attempt such studies for several sources at multiple frequencies. The recent developments of coherent dedispersion pipeline and wide-band digital backend system further facilitate the same.

1.3 Outline

The report presents an overview of the GMRT and the flow of signals from receivers to the storage devices in the next chapter. This is followed by a brief theoretical background on pulsars, the propagation effects suffered by radiation in the interstellar medium and several characteristics of individual pulses, in chapters 3 and 4. Chapter 5 discusses the properties of individual pulses of selected pulsars. Finally, chapter 6 concludes the report.

2 The GMRT: An Overview

The GMRT consists of an array of 30 antennas designed to operate at a range of frequencies from 50 MHz to 1450 MHz, each having a diameter of 45 m. Each dish is connected to a 'cradle' which is placed on the top of a 15 meter high concrete tower. The dishes have alt-azimuth mount. The antennas have been constructed using a novel technique nicknamed SMART (Stretched Mesh Attached to Rope Trusses). Their reflecting surface consists of panels of wire mesh which are attached to rope trusses, and by appropriate tensioning of the wires used for attachment the desired parabolic shape is achieved. This design has low wind loading, as well as low total weight for each antenna. Consequently, it was possible to build the entire array economically.

2.1 Array Configuration

Out of the 30 antennas comprising the GMRT, 14 are distributed randomly in a central region (~ 1 km across) called the central square. The antennas in the central square are labeled Cnn, with nn going from 00 to 14. The remaining antennas are distributed in a roughly Y shaped configuration, where each arm is ~ 14 km long. This provides a maximum baseline of ~ 25 km. The arms are called the 'East', 'West' and 'South' arms and the antennas in these arms are labeled E01...E06, W01...W06 and S01...S06 respectively. The array was originally meant to have 34 antennas, but was finally constructed with 30 due to escalating costs, resulting in missing numbers (C07, E01, S05) in the numbering sequence.

2.2 Receiver System

The GMRT currently operates at 5 different frequencies ranging from 150 MHz to 1420 MHz. Above this frequency range the antenna performance degrades rapidly because i) reflectivity of the mesh falls, and ii) aperture phase errors increase due to deviations of the plane mesh facets from a true parabola. The GMRT feeds, except for the 1420 MHz feed, are circularly polarized. None of the receivers are cooled; all of them operate at the ambient temperature. The feeds are mounted on four faces of a feed turret placed at the focus of the antenna. The 50 MHz feed is fixed to the feed support legs and not onto the turret. As such it is in focus at all times. The feed turret can be rotated to make any given feed point to the vertex of the antenna. The feed on one face of the turret is a dual frequency feed, i.e., it works at 233 MHz as well as 610 MHz. However, as part of a major upgrade this feed is getting replaced with a broad band feed covering 550 to 850 MHz. The schematic outline of a typical radio receiver system is shown in figure 1.

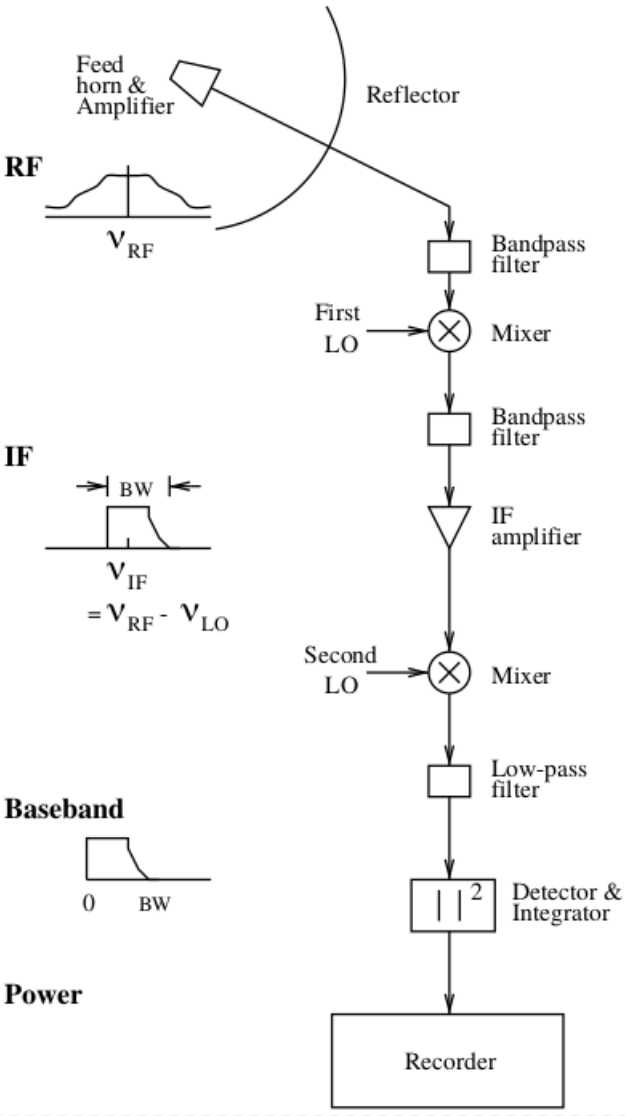

Figure 1: Schematic diagram of a Radio Telescope Receiver system. (Source: [6])

At the GMRT, the signals from all the feeds first pass through a RF amplifier, followed by a common second stage amplifier. The signals are then mixed with a suitable signal generated by a Local Oscillator (LO) in order to convert them to an Intermediate Frequency (IF). Each polarization is converted to a different IF and then fed to a laser-diode. The optical signals generated by the laser-diode are transmitted to the central electronics building (CEB) by fiber optic cables. At the CEB, they are converted back to electrical signals before being converted to baseband frequency by another set of mixers, and then fed into a suitable digital backend.

2.3 Digital Backends

The main backend for the existing legacy system is the GMRT software back-end (GSB). The GSB handles the full 32 MHz baseband signals from each of the two polarizations for all 30 antennas, which are digitized and sent to a networked cluster of PCs that perform all the operations needed to realize a correla-

tor and a pulsar receiver in real time. The GSB implements a FX correlator, which produces a maximum of 256 spectral channels for each of the two polarizations for each baseline. The GSB also has a beam former, running concurrently with the FX correlator, which produces incoherent array (IA) and phased array (PA) beam outputs for a user selectable set of antennas.

2.3.1 The GMRT Correlator

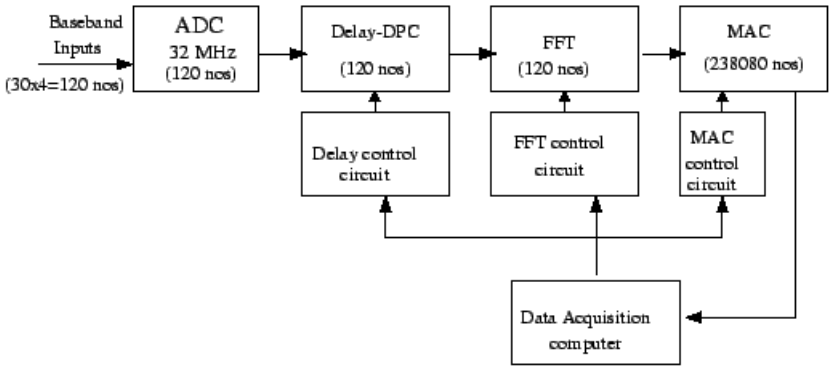

Figure 2: Simplified block diagram of the GMRT Correlator. (Source: [7])

A simplified block diagram of the GMRT correlator is shown in figure 2. Input at baseband frequency is first passed through ADCs, operating at a fixed clock frequency of 32 MHz. This implies that a signal with bandwidth of 16 MHz is Nyquist sampled. There are 120 ADCs, corresponding to two 16 MHz wide baseband signals for each polarization from 30 antennas. Following the digitization of the signals, they are passed through Delay-DPC unit, which compensates for delay accumulated due to varying distances of the antennas from the CEB. The signals are then converted from time domain to frequency domain by means of a FFT subsystem. Lastly, auto and cross-correlation operations are performed on these signals by a MAC unit and stored on a Data Acquisition Computer (DAC).

2.3.2 The GMRT Beamformer

Apart from the FX correlator, the GSB also consists of a beamformer, where the signals from the antennas can be combined to provide high time resolutions. Used chiefly for pulsar observations and study of radio transients, the beamformer supports Incoherent array (IA) and Phased array (PA) beam modes.

Coherently vs. Incoherently Phased Array

The signals from an n-element array can be combined in two ways: i) by adding the voltage signals from different antennas after proper delay and phase compensation, or ii) by adding the powers from different antennas. The former method corresponds to a coherent addition of signals whereas the latter

is an incoherent addition. The sensitivity to a point source is higher for the coherently phased array as compared to the incoherently phased array, by a factor of $\sqrt{n}$. The PA mode is therefore used to study individual radio sources. The IA mode is useful when the source is extended in size, since the beamwidth is much more than that of coherently phased array, resulting in better sensitivity in this case. It is also used when a large region of the sky is to be covered, for example, to search for new pulsars[7].

3 Pulsars: Theoretical Background

3.1 The magnetic fields of pulsars

Pulsars are highly magnetized, rapidly rotating neutron stars which emit radiation in a narrow cone centered around their magnetic axis. The misalignment between rotation and magnetic axes gives rise to lighthouse effect, and results in the observer receiving pulsating radio signals. The emission from the outer ring of the cone often dominates, resulting in a double pulse for some pulsars. The beam is locked onto the crust of the star by a strong magnetic field, which induces a local electric field and causes charged particles to be pulled out of the surface. Above the surface exists an ionized magnetosphere, co-rotating with the star out to a distance approaching r_c (=c/ω), which defines the 'velocity of light cylinder'[1].

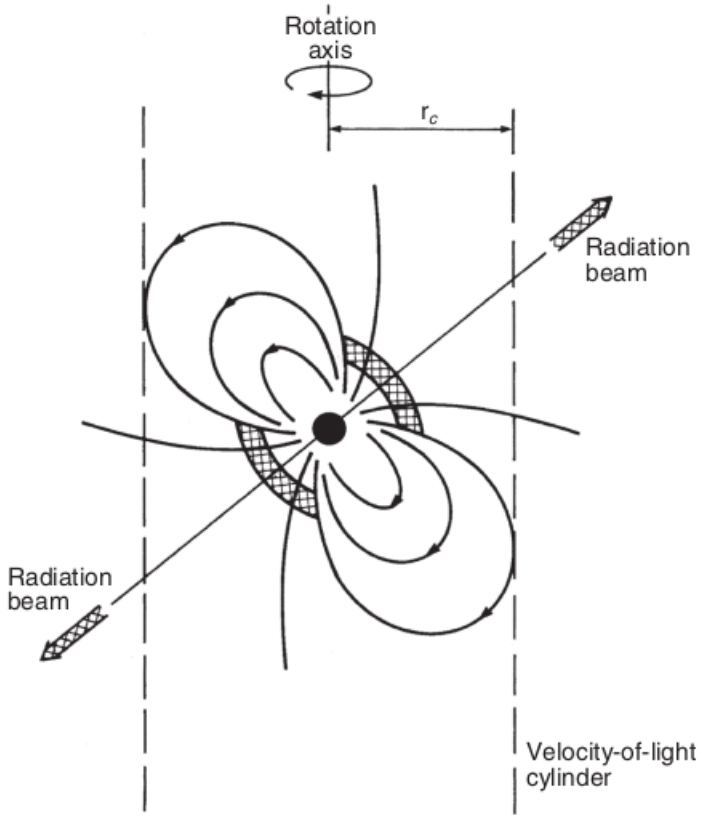

Figure 3: The pulsar magnetosphere. (Source: [1])

A schematic diagram of a pulsar magnetosphere is shown in figure 3. Once in the magnetosphere, these charged particles are accelerated along magnetic field lines, and emit synchrotron radiation. The condition in the magnetosphere is similar to the stellar interior, where there can be no net electric field. The static electric field in the magnetosphere is canceled by the induced electric field, such that

$$E + \tfrac{1}{c}(\Omega \times r) \times B = 0$$

The beam of radiation originates within the pulsar's magnetosphere. Radio emission is a small part of the total radiation emitted by pulsars. The radio beam originates above the stellar surface; the lower the

frequency, the further from the surface is the emitting region. High energy radiation originates in a separate region closer to the velocity of light cylinder[1].

3.2 Effects of the Interstellar Medium

The interstellar medium is the turbulent region between the stars, consisting of neutral atoms, ions, gas and dust. Radiation propagating through the medium encounters regions of variable refractive indices and compositions, causing the beam to deviate from its path. As a result, three distinct propagation effects occur, namely dispersion, scintillation and scattering. These effects and their observational consequences have been summarized below.

3.2.1 Pulse Dispersion

The group velocity of radio waves as they travel through the ISM depends on frequency, according to the relation

$$v_g = c\left[1 - \frac{n_e r_o \lambda^2}{2\pi}\right]$$

where $r_o = {e^2}/{mc^2}$ is the classical radius of the electron and n_e is the electron number density. The delay t in travel time over distance L as compared to free space is

$$t = \frac{n_e r_o c \nu^{-2}}{2\pi} L = 1.345 \times 10^{-3} \nu^{-2} n_e L \text{ seconds.}$$

The product $n_e L$ is known as the Dispersion Measure, and is a measure of total electron content between the source and observer. When quoting the frequency in megahertz, the delay becomes

$$t = 4.15 \times 10^3 DM\nu^{-2} \text{ seconds.}$$

Correction technique: De-dispersion

Due to dispersion in the interstellar medium, different frequency components of a pulse arrive at the receiver at different times. As a result, a receiver with bandwidth B_r (MHz) will stretch a pulse to a length

$$\Delta t = 8.3 \times 10^3 DM\nu^{-3} B_r \text{ seconds,}$$

which reduces the peak intensity of the pulse and consequently makes it difficult to observe pulsars with high DMs. In order to correct for dispersion, a technique known as de-dispersion is used. The receiver is divided into a number of frequency channels and the delay of each channel is calculated and corrected for by appropriate shifting. Finally, the signal is added together to obtain the de-dispersed pulse profile. The following figure shows pulse dispersion and its correction for the pulsar B1356-60 observed using the Parkes telescope[2].

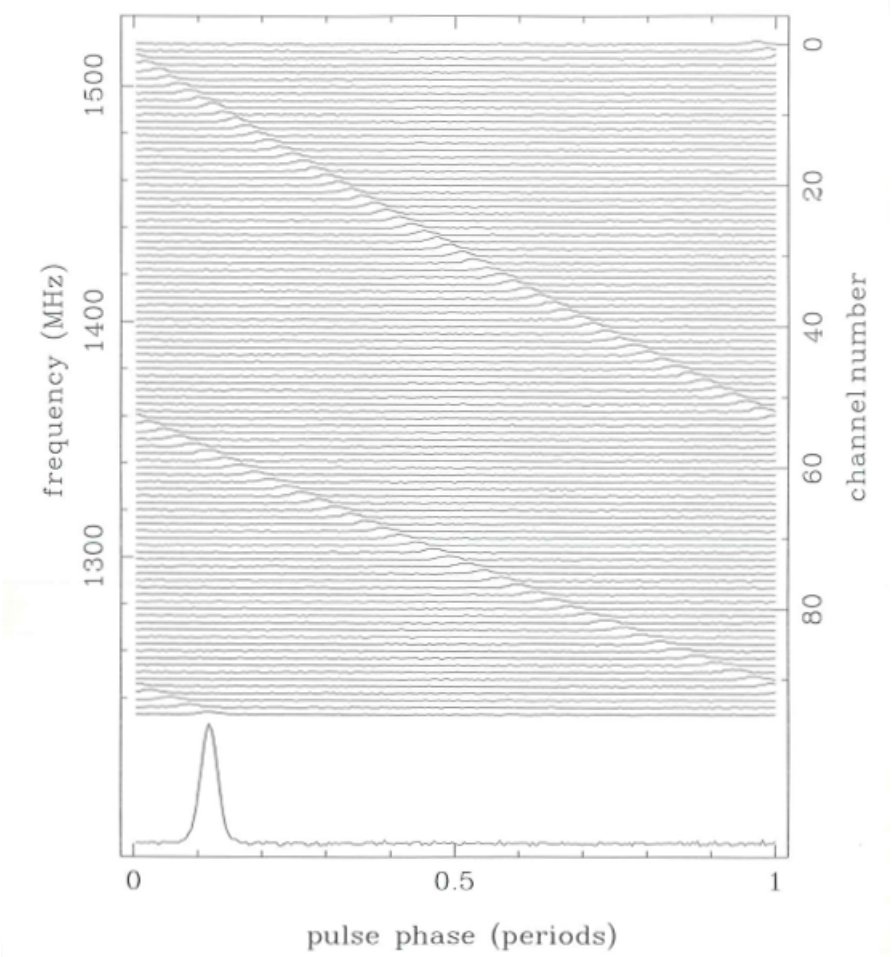

Figure 4: Pulse dedispersion. The frequency band is divided into 100 channels; the corrected profile is shown at the bottom. (Source: [2])

3.2.2 Scintillation

The turbulence in the ISM causes phase modulations on the propagating pulsar signal. These signals interfere with each other as their paths cross due to the varying refractive index of the medium. As a result, the observed intensity fluctuates over a variety of timescales and bandwidths. This effect, known as interstellar scintillation, is similar to twinkling of stars caused by disturbances in the Earth's atmosphere.

3.2.3 Scattering

Signals from distant pulsars are scattered by dust particles and irregularities in the ISM, which increases the path length of the rays and causes them to arrive at the receiver at different times. This delayed arrival of rays broadens an otherwise sharp pulse and reduces the signal to noise ratio, making it difficult to detect the pulsar. The scattering time, which quantifies the amount of scattering, is inversely proportional to the frequency of observation[2]:

$$\tau_s \propto {}^{1}/_{\Delta f} \propto f^{-4}$$

The strong frequency dependence favors observations carried out at higher frequencies.

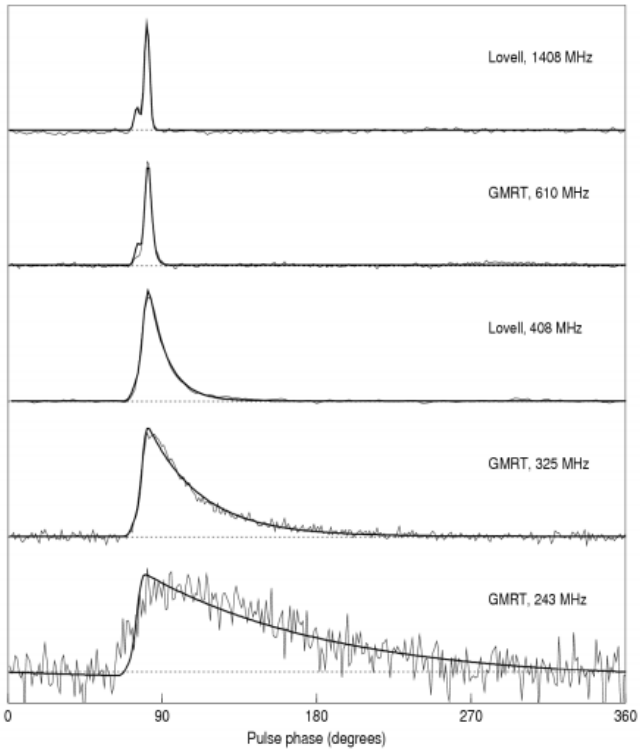

Figure 5: Pulse profiles for pulsar B1831-03 observed at five different frequencies. (Source: [2])

4 Characteristics of Individual Pulses

Pulsars are weak radio sources, and often the signal from several pulses must be added together in order to obtain a high enough signal to noise ratio. The structure of individual pulse profiles is inevitably lost in this process. However, with the rapid improvement in the techniques and instrumentation used in radio astronomy, individual pulse data from several pulsars can be studied without such integration. Individual pulses of pulsars show a variety of behaviors on different timescales. Several of these properties are discussed in this chapter.

4.1 Subpulses and Micropulses

The basic components of the pulse profile are known as subpulses, each having an approximately gaussian shape with typical widths of 10-20% of that of the integrated profile. One or more subpulses may be present in a pulse, each of which originates at a different radius in the emission cone. These subpulses may occur at the same, or at apparently random longitudes within the integrated pulse window. They may also drift systematically over this window, a phenomenon known as drifting. These subpulses further show intensity fluctuations over timescales of a few hundred microseconds. These 'micropulses' are considered to be modulations of the subpulse radiation itself, instead of being distinct components of emission.

4.2 Pulse Nulling

Some pulsars exhibit an abrupt decrease in the pulse intensity (to about 1% of the mean power) for several periods before reverting to normal. This phenomenon, known as pulse nulling, was first reported by Backer in 1970. The length of the nulls, as well as the interval between their occurrences vary from one pulsar to another. Nulling indicates faltering of the emission process and is typically observed in older pulsars. Nulling may not occur simultaneously at all frequencies of observation, indicating the presence of emission processes which are preferential at certain frequencies. Most nulling pulsars are found in the $P-\dot{P}$ diagram (figure 6) close to the death line. The pulsars approaching this line from the left are nearing the end of their active lives. It is observed that the total power radiated by a pulsar decreases with age, which could be related to a decrease in rotation rate, and/or due to a decay of the dipole magnetic field[1].

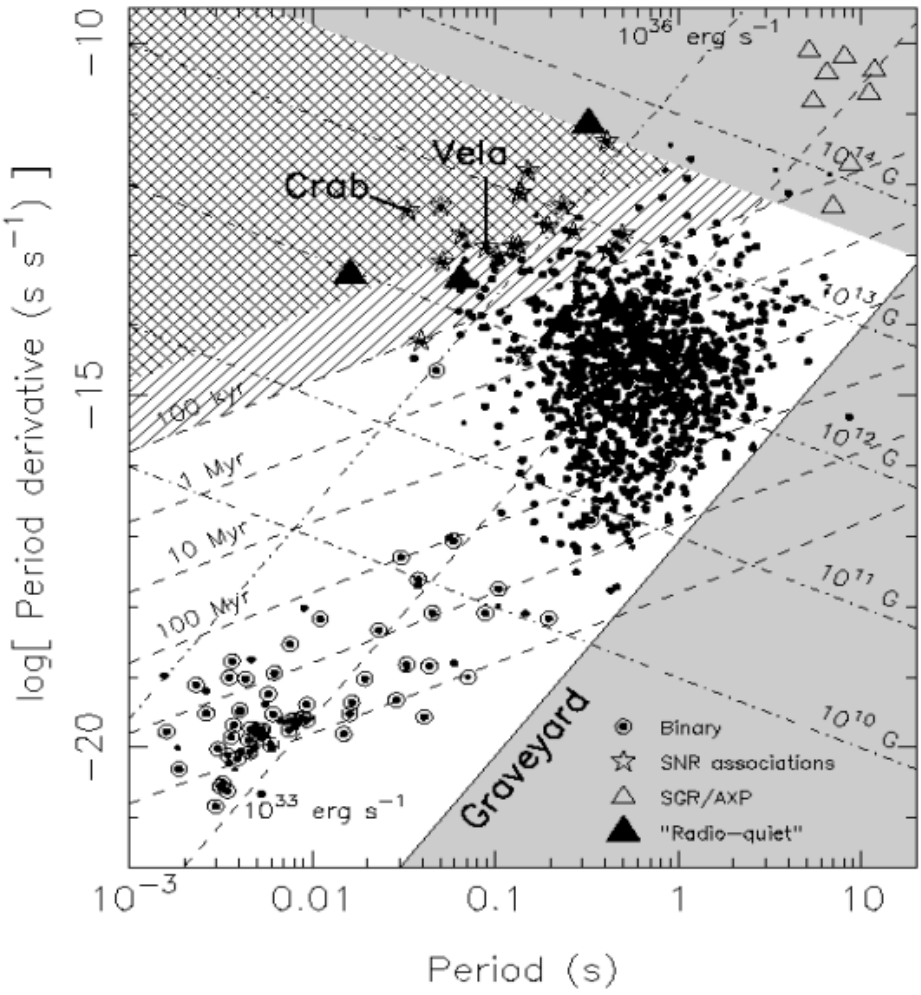

Figure 6: Logarithmic plot of period P against its derivative $\dot{P}$. (Source: [2])

4.3 Drifting Subpulses

The subpulses of some pulsars occur at progressively changing longitudes across the window defined by the integrated profile. A longitude-time diagram used to describe this phenomenon shows well organized bands of subpulses. Subpulses from two adjacent bands are commonly found within a given individual pulse; the separation between these is known as the secondary period, P2. Another characteristic is the spacing between adjacent bands, known as band spacing, P3. A schematic representation of drifting subpulse phenomenon is shown in figure 7.

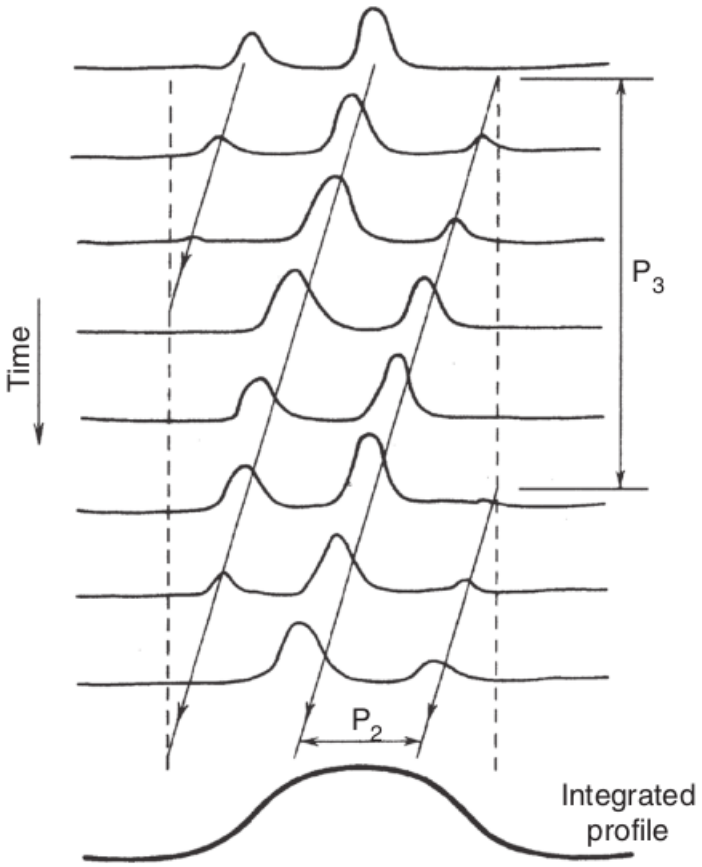

Figure 7: Description of drifting subpulse phenomenon. (Source: [4])

Both drifting and nulling are more commonly found in older pulsars. In case of pulsars which exhibit both these phenomena, it is observed that the drift is unaffected by the null, i.e., drift resumes from a longitude 'remembered' from the time when the null started. This suggests that these two behaviors are indeed correlated. The following chapter provides details of the analysis performed as part of this project.

5 Analysis

The data obtained from the GMRT is saved in a .raw format. The GMRT Pulsar Tool, or GPTool as it is more often referred to, is employed to dedispersed the data and produce the folded profile. The file used to set up GPTool (gptool.in) takes several inputs from the user, including the number of frequency channels to use for dedispersion, and the name of the pulsar, which it then searches for in the ATNF Pulsar Catalog to obtain the period and DM of the pulsar. In addition to this, it also filters the data to some extent, removing outlying peaks and hence reducing radio frequency interference (RFI) to some extent. One of the outputs of GPTool is a timeseries, which contains intensity vs. time data after dedispersion. Prior to the beginning of this project, a C code was available to analyze the dedispersed timeseries and browse through individual pulses. The routine allowed the user to find pulses with SNR greater than a threshold value, integrate adjacent samples of the data, and to plot auto-correlation of any pulse. As part of the work done during this project, the following features have been added to the existing C code.

Energy Histograms The option to plot energy histograms can be used to check for the presence of nulling and subsequently, with the help of another routine written in Python, calculate the nulling fraction for a pulsar. The user enters the number of pulses for which the histograms have to be plotted, and the number of histogram bins. The routine calculates the energy in the on-pulse region (which is defined by the user once the routine starts) and the energy in a window of the same size in the off-pulse region, and afterwards saves the values in a text file. The routine also plots the two histograms -corresponding to on-pulse and off-pulse energies- using PGPLOT.

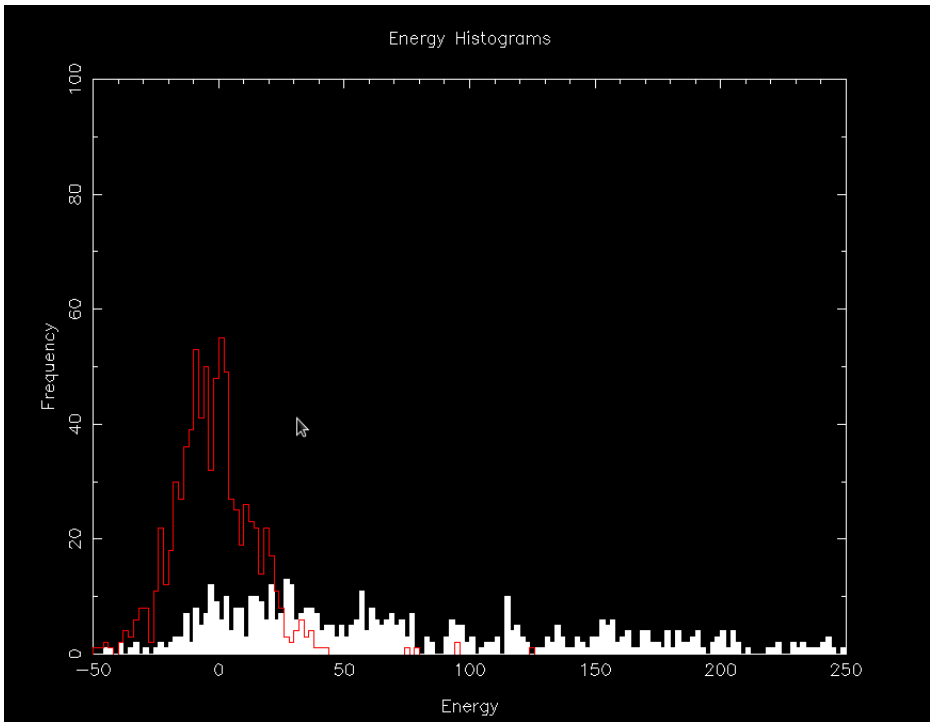

Figure 8: On-pulse (white) and off-pulse (red) energy histograms for PSR B1742-30

If nulling is present, the on-pulse energy histogram shows a bump at zero energy. An example of such a plot for pulsar B1742-30 is shown in figure 8. The on-pulse energy has a peak at zero energy and another at ~30. By comparing the height of this bump in the on-pulse histogram with the height of the off-pulse histogram, one can get an estimate for the nulling fraction of the pulsar. Another routine written in Python, is used to calculate the nulling fraction in the following way. A fraction of the off-pulse histogram is subtracted from the on-pulse histogram such that the bump at zero energy disappears. The fractional value that achieves this is the nulling fraction of the pulsar. The nulling fraction for the B1742-30 is calculated using this method in the next chapter.

Grayscale Plots This option allows the user to plot intensities of a number of subsequent pulses as a function of longitude as a 2-dimensional grayscale plot using PGPLOT. The user enters the phase range to be plotted on the x-axis, as well as the number of bins it should be divided into, followed by the number of pulses to be plotted and the starting pulse number. An example of the resulting grayscale plot is shown in figure 9. The plot proves to be useful when investigating for drifting subpulses in a pulsar, which can be clearly seen as dark bands (corresponding to greater intensity) on a light background.

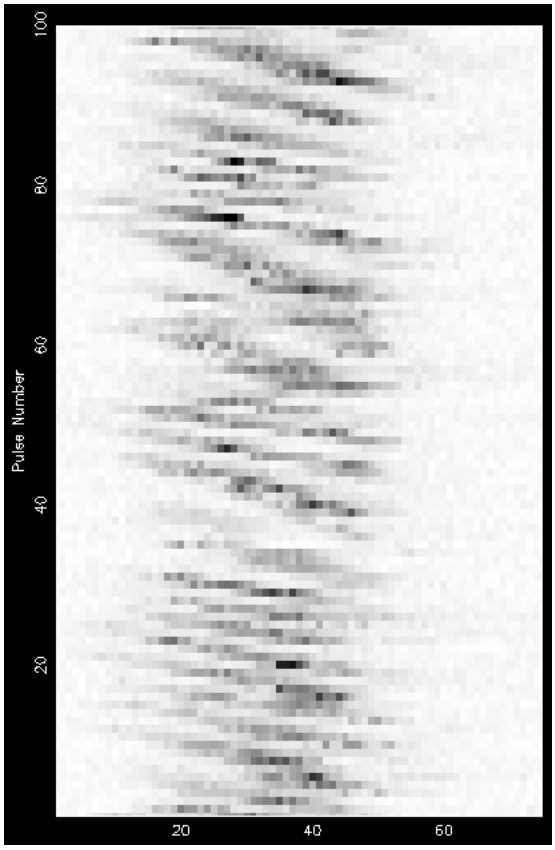

Figure 9: Grayscale plot showing drifting subpulses in PSR B2016+28

6 Results and Discussion

Individual pulse data from several pulsars observed via the GMRT were analyzed during the course of this project. These pulsars, their parameters and observational details are tabulated below (Table 1). The properties exhibited by these pulsars are discussed in the following sections.

Table 1: Observational parameters of discussed pulsars

PSR	**DM** (pc/cm^{-3})	**Period (s)**	**Obs. Freq. (MHz)**	**BW (MHz)**	**Sampling time** (μs)
B2016+28	14.197	0.558	325/610	32/200	15.36/40.96
B1742-30	88.373	0.367	650	200	5.12
J2145-0750	8.997	0.016	400/650	200	5.12

6.1 PSR B2016+28

B2016+28 is one of the pulsars in which the phenomenon of drifting subpulses was first observed by Drake and Craft in 1968. The longitude-time diagram in figure 10 shows well organized bands of drifting subpulses. The secondary period P_2 is reported to be around 7 degrees of longitude, while the band spacing P_3 varies from 3 to 15 periods[9]. Consequently, the band slope $|D_\phi| = {}^{P_2}/_{P_3}$, also varies considerably from one band to another.

The drifting subpulses were observed at two different frequencies by conducting simultaneous multi-frequency observations via two available backends; the GMRT Software Backend (325 MHz) and the GMRT Wide-band Backend (610 MHz). As reported in the paper by Naidu *et al.*, 2018[3], the drift bands are correlated across the two frequencies, leading to the conclusion that drifting is independent of frequency of observation. The pulsar does not show any significant nulling.

Rough estimates for P_2 and P_3 were made by observing the drift bands in the longitude-time grayscale plots. The secondary period comes out to be approximately 8 degrees of longitude. A similar calculation yields a value between 5 to 20 pulse periods for the band spacing. Both of these figures are in agreement with the ones previously reported in literature[9].

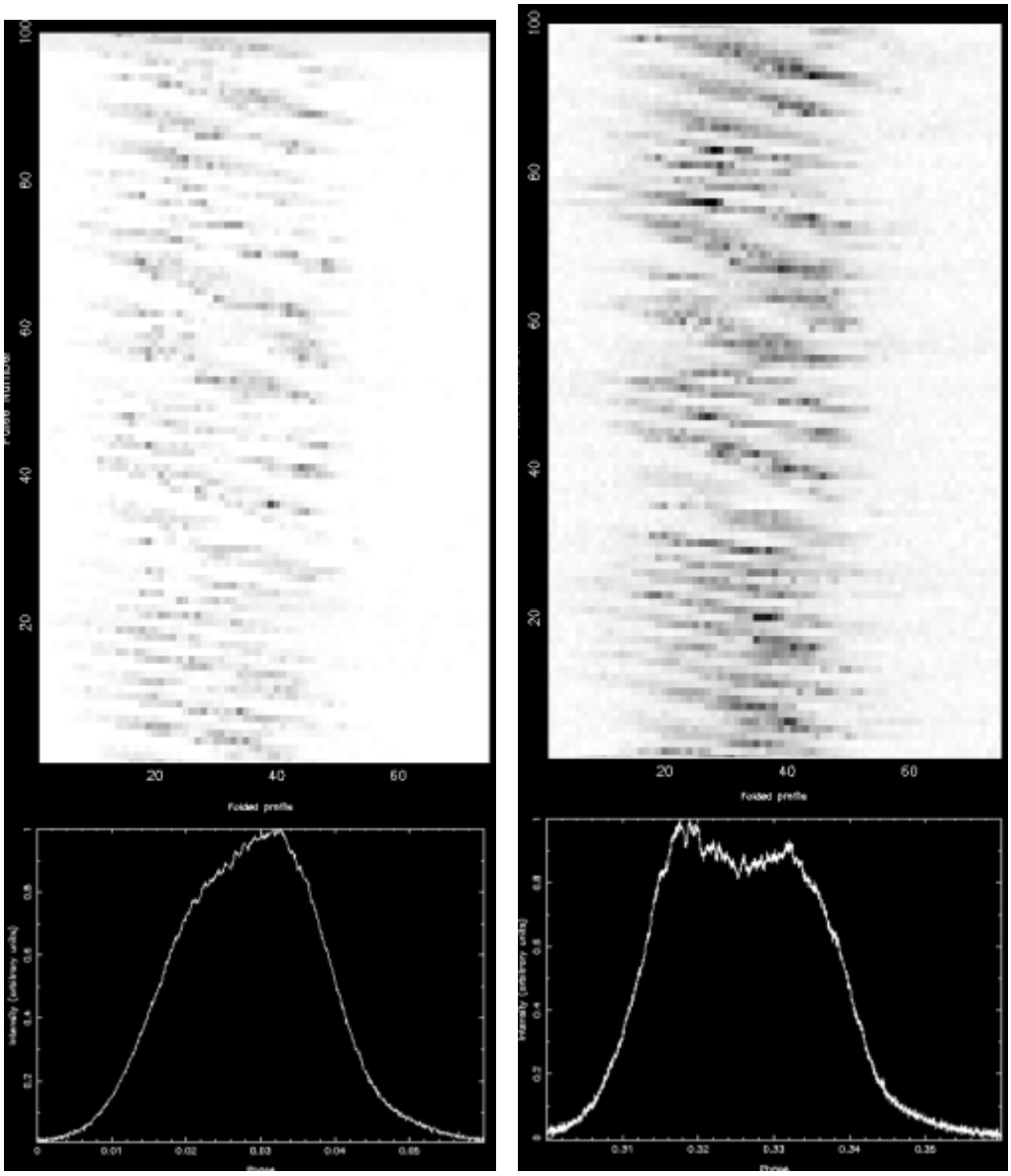

(a) 325 MHz (b) 610 MHz

Figure 10: Longitude-time diagrams for pulsar B2016+28

6.2 PSR B1742-30

This pulsar was observed via the GMRT over a frequency band of 550 MHz to 750 MHz. The raw data was dedispersed via the coherent dedispersion pipeline. The pulsar is known to show pulse nulling, and has a previously reported nulling fraction of ~25%[8]. A grayscale plot of about 800 pulses of this pulsar (figure 11) shows strong pulses for a number of periods, followed by little or no emission for several periods. The plot does not show any systematic motion of subpulses across the pulse window, and hence we conclude that the pulsar does not exhibit the phenomenon of drifting subpulses.

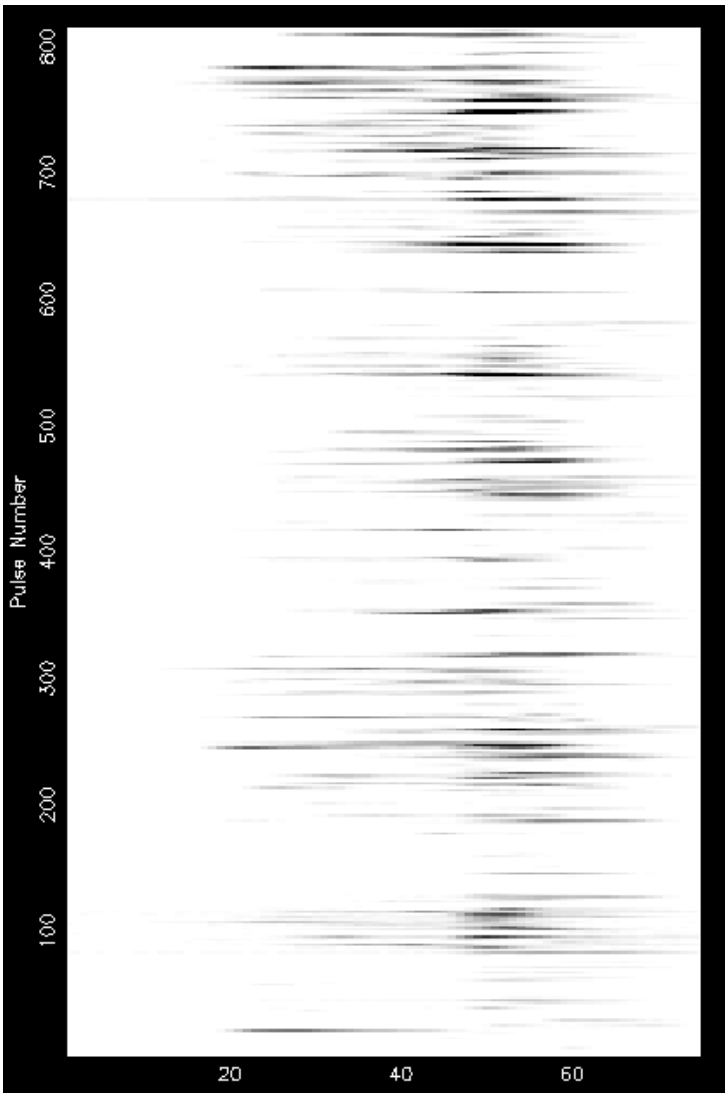

Figure 11: Randomly distributed subpulses in PSR B1742-30

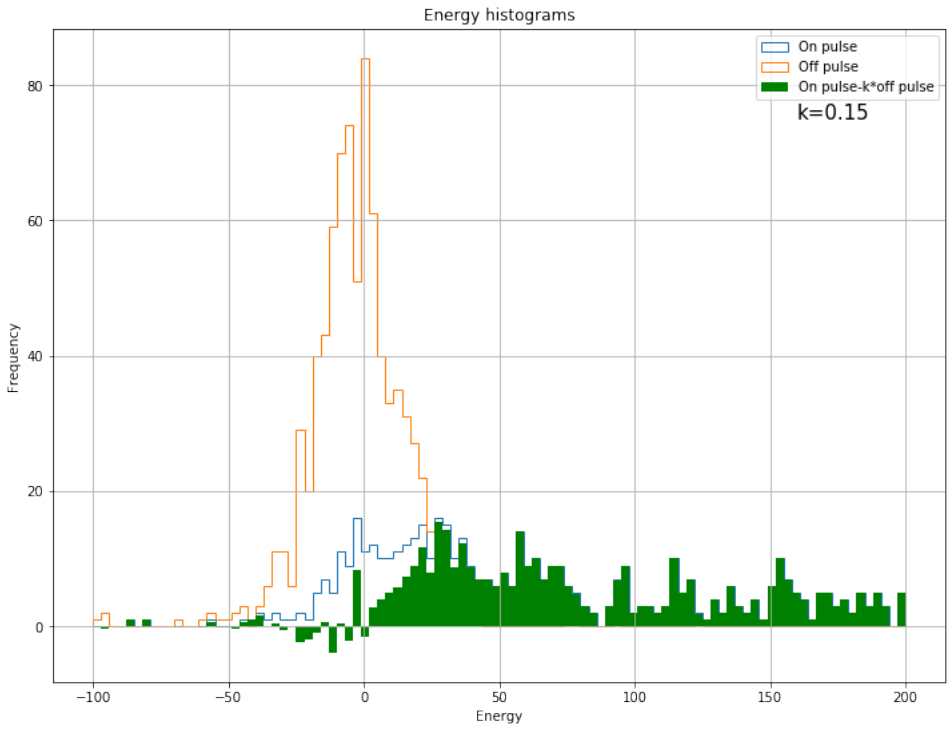

Figure 12: Energy Histograms for pulsar B1742-30

The on pulse and off pulse energy histograms for this pulsar are shown in figure 12. The nulling fraction of the pulsar was calculated by subtracting histograms, as explained in the previous chapter. The value of the fraction was adjusted such that there are minimum number of bins with energy at and/or close to zero, while keeping in mind that the frequency cannot take a negative value. The estimated nulling fraction is around 15%, close to the value reported in literature.

6.3 PSR J2145-0750

J2145-0750 is different from the two previously mentioned pulsars in that it is a millisecond pulsar, with a period of about 16 ms. Millisecond pulsars are distinguished from 'normal' pulsars by their small periods, usually less than 30 ms, as well as their small spin down rates. They also have a high probability of being found in a binary system. The presence of a companion justifies the high spin periods via the following evolutionary scenario. Starting from two main sequence stars, we assume that the initially more massive (primary) star evolves first and undergoes a supernova to form a neutron star. Assuming that the binary system is not disrupted by the explosion, the neutron star spins down as normal pulsar for the next million years. At some later time, the second star begins its red giant phase, at which point, the strong gravitational pull of the neutron star attracts matter from its companion. The accretion of matter transfers orbital angular momentum to the neutron star, spinning it up to extremely small periods and also reducing its magnetic field (which is proportional to $\sqrt{P\dot{P}}$). As a result, pulsars with short periods and period derivatives are born[2].

The data for the pulsar J2145-0750 was obtained via the coherent dedispersion pipeline, with a sampling time of 5.12 μs. Sampling times of this order are necessary to resolve the pulses of millisecond pulsars as their periods are relatively short. The data was recorded in two frequency bands - Band 3 (300 MHz to 500 MHz) and Band 4 (550 MHz to 750 MHz). The folded profiles in the two bands are shown in figure 14. The folded profile in both the bands has two distinct components, emanating from two different regions inside the emission cone. However, the relative intensities of the two vary significantly. In Band 3, the leading component is almost equal to the trailing one, which suggests that both regions emit equal amount of flux in this band. On the other hand, in Band 4 the leading component is much stronger than the trailing component, suggesting that one region emits more strongly at higher frequencies compared to the other. The energy histograms (figure 13) for this pulsar are well separated, implying that the nulling fraction is small (<10%).

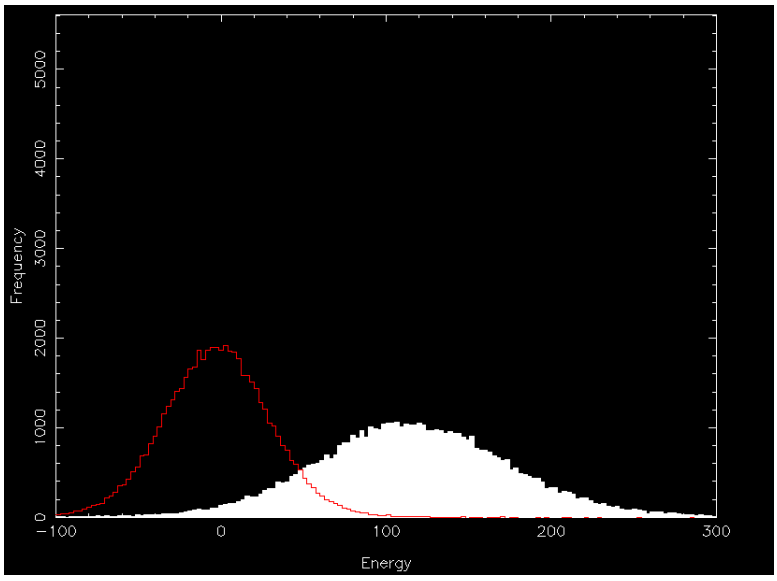

Figure 13: On-pulse (white) and off-pulse (red) energy histograms for PSR J2145-0750

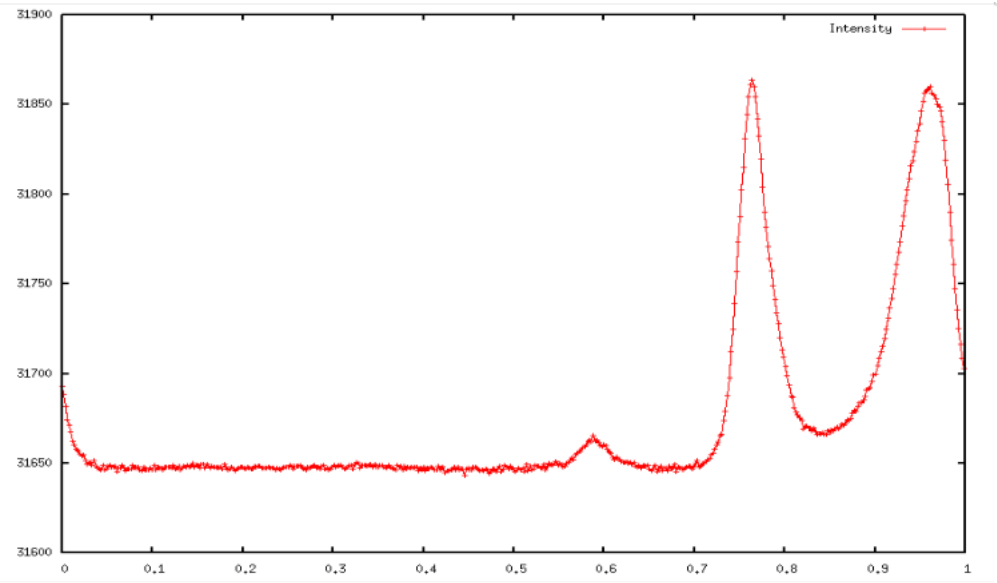

(a) Band 3

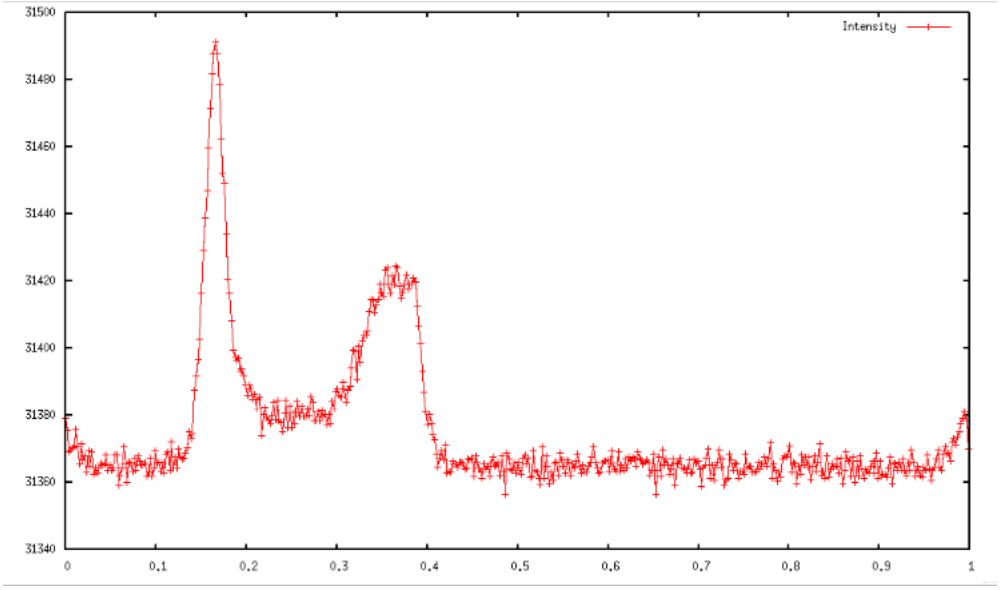

(b) Band 4

Figure 14: Folded profiles of J2145-0750 in Bands 3 and 4

Individual pulses of the pulsar are much narrower than the folded profile and show the expected, approximately gaussian shape. Figure 15 shows a typical strong pulse in two frequency bands with bandwidths of 100 MHz each and central frequencies of 600 MHz and 700 MHz respectively. The emission in the lower half band is stronger than that in the upper half band owing to the inverse relationship between flux emitted by the pulsar and the frequency of observation.

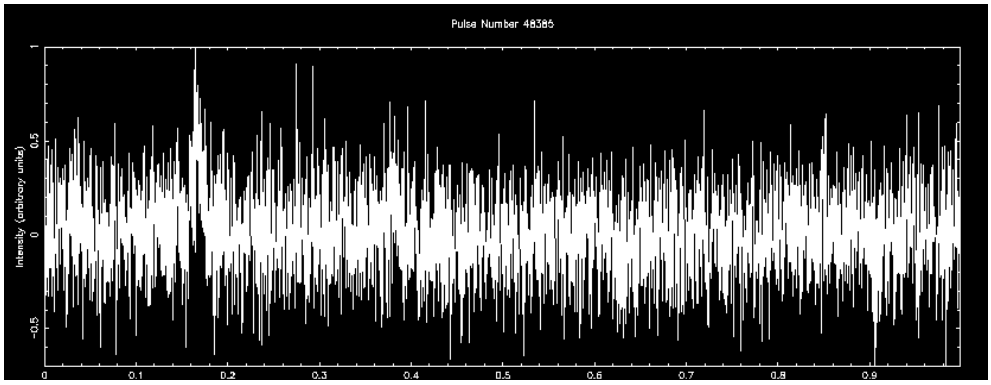

(a) Pulse 48385 in lower half band

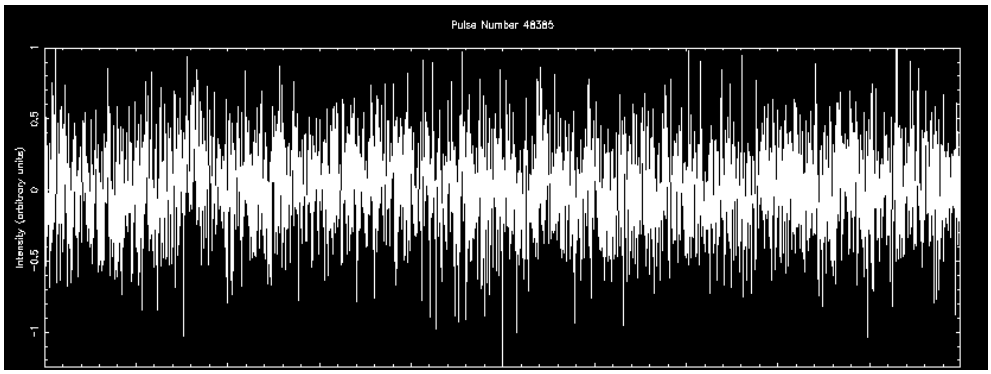

(b) Pulse 48385 in upper half band

Figure 15: Variation of pulse profile with frequency

RFI or Giant Pulses?

Giant pulses are nanosecond bursts of emission with intensity up to 1000 times that of an individual pulse. In high resolution timeseries, they are observed as sharp spikes in the pulse window. A similar structure was observed in some of the pulses in band 4 data of PSR J2145-0750 (figure 16). However, the presence of such spikes in the pulse window does not imply giant pulse emission, because a similar structure is often exhibited by RFI. The authenticity of this feature can be verified by virtue of the broadband nature of pulsar emission. Pulsars emit over the entire range of frequencies, while RFI are unlikely be present over a wide frequency band. In order to perform this test, band 4 was divided into two sub-bands - 550 MHz to 650 MHz and 650 MHz to 750 MHz, using GPTool. The same pulse number was then observed in the two sub-bands, as shown in figure 16.

The spikes are seen in the lower half band, but not in the upper half band. This leads to the conclusion that the spikes are indeed RFI, and not giant pulses, since the latter would be present over the entire band and not just in the lower half band.

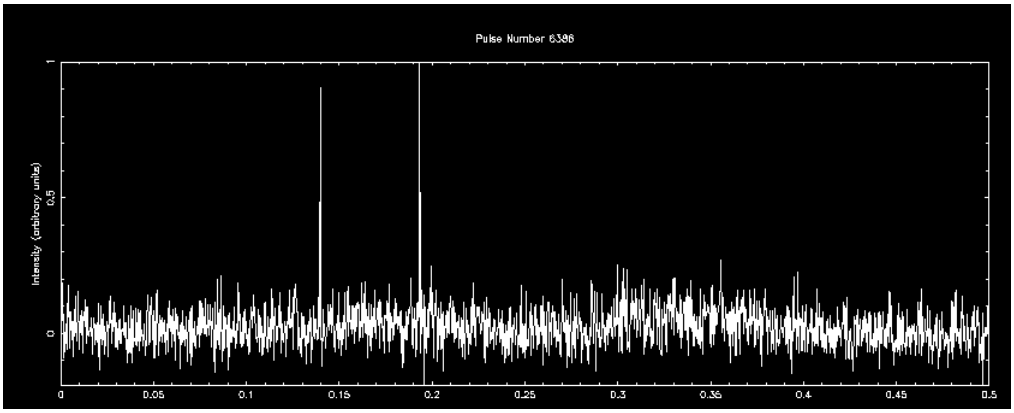

(a) Lower Sub-band (550 MHz to 650 MHz)

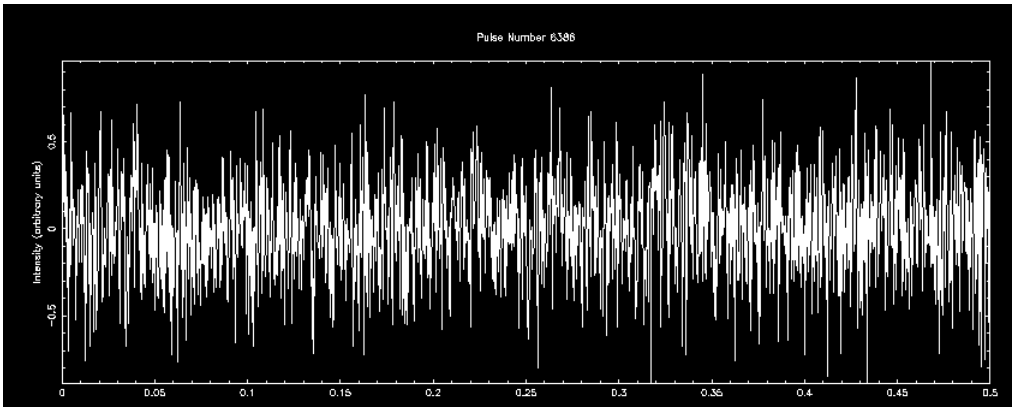

(b) Upper Sub-band (650 MHz to 750 MHz)

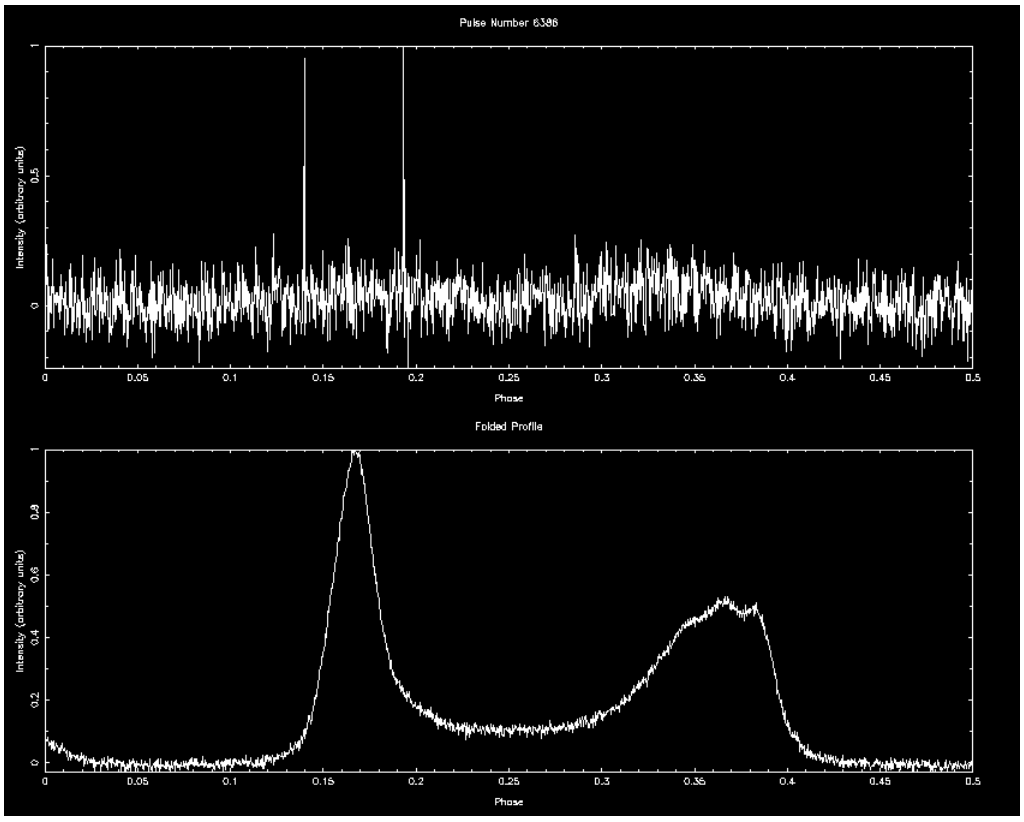

(c) Full Band (550 MHz to 750 MHz)

Figure 16: Pulse number 6386 of PSR J2145-0750

7 Conclusion

The preceding chapters discussed some of the characteristics of single pulse profiles of several pulsars. During the course of this project, individual pulse data from three pulsars was analyzed. The methods employed to analyze these behaviors has also been elaborated in this report. However, much remains to be done. In order to achieve a thorough understanding of the emission mechanism one needs to study the properties of more such pulsars and find possible correlations between them. More pulsars should be analyzed for pulse nulling in order to find a definite correlation between the age of pulsar and the faltering emission mechanism. In the case of nulling in pulsar B1742-30 presented earlier, approximately 800 pulses were used to plot the histograms. With more pulses, that is, by conducting longer observations, the two peaks in the on-pulse histogram can be brought out more distinctly. Similarly, one needs more data on pulsars with drifting subpulses in order to learn more about the emission regions within the radiation cone.

By carrying out detailed investigations of the pulsar phenomenon using highly sensitive instruments such as the GMRT, one can uncover the mysteries of the exotic objects that are pulsars.

Acknowledgments

I wish to express my sincerest gratitude to Prof. Yashwant Gupta, for providing me this opportunity to work in the wonderful field of pulsar astronomy and for his immense counsel throughout the course of this project. Without his continual guidance and motivation, I would not have been successful in this endeavor. I also want to thank the members of the staff at NCRA and GMRT as well as other summer students for their constant support and encouragement for the past two months.

References

[1] Lyne & Graham-Smith. (1990) *Pulsar Astronomy.* Cambridge: Cambridge University Press.

[2] Lorimer and Kramer. (2005) *Handbook of Pulsar Astronomy*. Cambridge: Cambridge University Press.

[3] Naidu, A., Joshi, B. C., Manoharan, P. K., and KrishnaKumar, M. A. (2017). Simultaneous multi-frequency single pulse observations of pulsars. *A&A,* 604, A45.

[4] Allen, M. C., Melrose, D. B. (1983). Drifting Subpulses in Pulsars. *ASA,* 5(2), 191-195.

[5] Gajjar, V., Joshi, B.C., and Kramer, M. (2012). A survey of nulling pulsars using the Giant Meterwave Radio Telescope. *Monthly Notices of the Royal Astronomical Society*, 424, 1197-1205.

[6] Bhattacharya, D. (1998). Detection of Radio Emission from Pulsars: a Pulsar Observation Primer. *The Many Faces of Neutron Stars,* 103-128.

[7] Chengalur et al. (2007) *Low Frequency Radio Astronomy*. NCRA-TIFR, Pune.

[8] Basu, R., Mitra, D., and Melikidze, G. I. (2017). Meterwavelength Single-pulse Polarimetric Emission Survey III: The Phenomenon of Nulling in Pulsars. *The Astrophysical Journal*, 846(2), 109.

[9] Taylor, J. H., Manchester, R. N., and Huguenin, G. R. (1975). Observations of pulsar radio emission. I - Total-intensity measurements of individual pulses. *The Astrophysical Journal*, 195, 513